journal of the mechanical behavior of biomedical materials 136 (2022) 105480

Contents lists available at ScienceDirect

Journal of the Mechanical Behavior of Biomedical Materials

journal homepage: www.elsevier.com/locate/jmbbm

L-DOPA coating improved phosphate glass fibre strength and fibre/matrix interface

Chao Tan [a], Chris D. Rudd [b], Andrew J. Parsons [c], Nusrat Sharmin [d], Ifty Ahmed [e,*]

[a] College of Materials Science and Engineering, Sichuan University, Chengdu, 610065, China
[b] James Cook University, 387380, Singapore
[c] Composites Research Group, Faculty of Engineering, University of Nottingham, Nottingham, NG7 2RD, UK
[d] Department of Processing Technology, Nofima AS, Richard Johnsens Gate 4, 4021, Stavanger, Norway
[e] Advanced Materials Research Group, Faculty of Engineering, University of Nottingham, Nottingham, NG7 2RD, UK

ARTICLE INFO

Keywords:
L-DOPA
Coating
Phosphate glass fibre
Fibre/matrix interface
Fibre strength

ABSTRACT

The levodopa (L-DOPA) has been reported as a promising adhesive for various materials. In this study, we utilized L-DOPA as an interfacial agent for phosphate glass fibre/polycaprolactone (PGF/PCL) composites, with the aim to enhance the interfacial properties between the fibres and polymer matrix. The PGFs were dip-coated in varying concentrations of L-DOPA solution ranging between 5 and 40 g L^{-1}. The fibre strength and interfacial shear strength (IFSS) of the composites were measured via a single fibre tensile test and single fibre fragmentation test, respectively. It was found that the L-DOPA agent (at conc. 10 g L^{-1}) significantly improved the IFSS of the composites up to 27%. Also, the L-DOPA coating (at conc. 40 g L^{-1}) significantly increased the glass fibre strength up to 18%. As a result, an optimum coating level could be tailored depending on application and whether fibre strength or IFSS was of greater importance. In addition, SEM and TGA analyses were used to detect and quantify the coating agents. FTIR and XPS further confirmed presence of the coating and indicated the zwitterionic crystals of L-DOPA and the formation of a melanin-like polymer layer. The spectroscopy data also evidenced that both catechol and amine groups contributed to the interaction between the L-DOPA and the PGF surface.

1. Introduction

Traditionally, metals have been used for bone fracture fixation devices due to their excellent mechanical properties. However, a secondary surgery is usually needed to remove those implants after treatment. Meanwhile, the high mechanical properties of metals can also lead to "stress-shielding" effects (Ambrosi et al., 2021). Therefore, many studies have focused on resorbable fibre-reinforced composites as a substitute for metal implants in bone tissue engineering along with adequate toughness and good biocompatibility (Tan et al., 2018a; Felfel et al., 2021). The reinforcement of resins with short or long fibres has multiple applications in various biomedical fields, especially in medicine and Dentistry (Lin et al., 2020). However, the application of polymer composites, such as phosphate glass fibre/polycaprolactone (PGF/PCL), is limited by the rapid degradation of mechanical properties after exposure to an aqueous physiological environment, which is attributed to loss of their interfacial properties (Tan et al., 2018a; Felfel et al., 2021). Coupling agents have been explored to improve the interfacial properties of the fibre/polymer composites but with limited success (Tan et al., 2018a; Felfel et al., 2021).

The mussel adhesive proteins (MAPs) of marine mussels are able to form adhesive "feet" to attach to almost all kinds of materials in humid environments (Quan et al., 2019). 3,4-dihydroxy-l-phenylalanine (L-DOPA) is an important constituent of the adhesive foot protein (Mefp-5, Mytilus edulis foot protein-5) found near the plaque-substrate interface of mussels, which plays a central role in strong adhesion of mussels onto a wide range of organic and inorganic substances (Quan et al., 2019; Lee et al., 2007). The catechol units were found to be responsible for the adhesive properties of L-DOPA and the catechol-containing molecules and polymers have been applied to coat various materials including metals, ceramics/glasses and polymers (Quan et al., 2019; Cheng et al., 2022). Additionally, there have been

* Corresponding author.
E-mail addresses: tanchao@scu.edu.cn (C. Tan), chris.rudd@jcu.edu.au (C.D. Rudd), andrew.parsons@nottingham.ac.uk (A.J. Parsons), nusrat.sharmin@nofima.no (N. Sharmin), ifty.ahmed@nottingham.ac.uk (I. Ahmed).

https://doi.org/10.1016/j.jmbbm.2022.105480
Received 10 June 2022; Received in revised form 16 September 2022; Accepted 18 September 2022
Available online 27 September 2022

multiple attempts to utilize the adhesive properties of L-DOPA for materials applied in various biomedical fields, such as gene delivery and bone repair (Lee et al., 2013). The catechol groups in L-DOPA have the capacity to form hydrogen bonds, metal-ligand complexes, and quinhydrone charge-transfer complexes, which enable a strong adhesion to various types of materials (Jo et al., 2018). Further, the carboxyl and amine groups enable L-DOPA to react with other organic materials. Therefore, L-DOPA shows the potential as a coupling agent for PGF/PCL composites in biomedical applications.

In addition, L-DOPA is one of the precursors of eumelanin synthesis. Eumelanin is naturally formed with L-DOPA or tyrosine as precursors (Quan et al., 2019; Lee et al., 2019). The Raper-Mason pathway is the most universal and well-known route for the synthesis of eumelanin and Fig. 1 shows the schematic representation of the pathway (Lee et al., 2019). The first step involves the catalytic- or auto-oxidation of L-DOPA to dopaquinone. Dopaquinone is a highly reactive intermediate and converts to leucodopachrome by a rapid spontaneous autoxidation, which is then reversibly oxidized to dopachrome. Dopachrome converts to 5,6-dihydroxyindole-2-carboxylic acid (DHICA) and may further evolve to 5,6-dihydroxyindole (DHI) by decarboxylation. Further oxidation of these dihydroxyindoles results in indolequinones and subsequent crosslink reactions between hydroxyl and quinone forms lead to polymerization (Quan et al., 2019).

This study investigated the feasibility of L-DOPA as a coupling agent for PGF/PCL composites. Surface morphology observation (SEM), thermogravimetric analysis (TGA) and surficial chemical analysis (FTIR and XPS) were conducted to detect and quantify the L-DOPA coating on PGF surface and also to investigate the chemical interaction between L-DOPA and PGFs. Then, mechanical properties of the uncoated and coated PGFs were ascertained using a single fibre tensile test (SFTT). The interfacial shear strength (IFSS) was analyzed using a single fibre fragmentation test.

2. Materials and methods

2.1. Glass fibre preparation and coating application

Continuous phosphate glass fibres (PGF, $45P_2O_5$–$5B_2O_3$–$5Na_2O$–24CaO–10MgO–$11Fe_2O_3$ in mol%) of ~25 μm diameter were prepared as described previously (Tan et al., 2018b).

A coating solution was prepared by dissolving 3,4-Dihydroxy-*L*-phenylalanine powders (L-DOPA, ≥ 98% TLC) of different quantities (PDP-0.5, 1, 2 and 4) in 0.01 M Tris buffered saline solution (TBS, pH 8.5 ± 0.1 at 24 °C) and catalysing by $NaIO_4$ solution (10 g/L). All the chemicals were purchased from Sigma Aldrich, US.

The prepared PGFs were dip-coated in the L-DOPA solution for 30 min before a gentle washing in deionised water to remove non-adhered material. Then, the coated PGFs were dried in an oven at 37 °C overnight. Uncoated PGFs were also placed in the oven and prepared as a control, which was named as PDP-0. Details of the five different coating conditions are shown in Table 1.

2.2. Coating performance analysis

Scanning electron microscopy (Sigma/VP SEM, Zeiss, Germany) and infrared spectroscopy (Vertex 70 FTIR-ATR, Bruker, Germany) were used to detect the L-DOPA coating on a PGF surface.

Thermogravimetric analysis (SDT Q600, TA Instruments, US) was conducted to detect and quantify the coating material. PGF samples were heated from room temperature to 450 °C, which is below the glass transition temperature (T_g) of the PGF (which is 520 ± 5 °C) (Tan et al., 2017). A heating rate of 20 °C min^{-1} in flowing nitrogen gas of 50 mL min^{-1} was used for the experiment.

X-ray photoelectron spectroscopy (XPS) was used to investigate the chemical interaction between L-DOPA and PGF surface. An Axis Ultra (Kratos, UK) with a monochromated AlK_α X-ray source (1486.6 eV) was operated at 8 mA emission current and 12 kV anode potential. For the XPS measurement, a fibre bundle was mounted on the sample stage using conductive adhesive tape at both ends, while the L-DOPA powder was adhered on the stage by using conductive tape. Drift of the electron binding energy of the peaks caused by surface charging was calibrated by using the C_{1s} peak of the C–C bond at 284.5 eV.

2.3. Fibre strength measurement

The effect of coating application on mechanical properties of PGFs was analyzed via the single fibre tensile test (SFTT) using a LEX 820 tensile tester (Diastron, UK) in accordance with ISO 11566. Thirty samples were tested for each subject. Weibull distribution was used to characterise the failure mode of the brittle PGFs and the data was processed by using Minitab 17 software. More operating details are shown in (Tan et al., 2018a).

Table 1
Details of coating application. The sample codes were also used for the corresponding single fibre composites. "PDP" means PGF-DOPA-PCL.

Sample codes	Units	PDP-0	PDP-0.5	PDP-1	PDP-2	PDP-4
TBS solution	mL	–	100	100	100	100
L-DOPA	g	–	0.5	1	2	4
Dip-coating at RT	min	–	30	30	30	30
Drying at 37 °C	hour	24	24	24	24	24

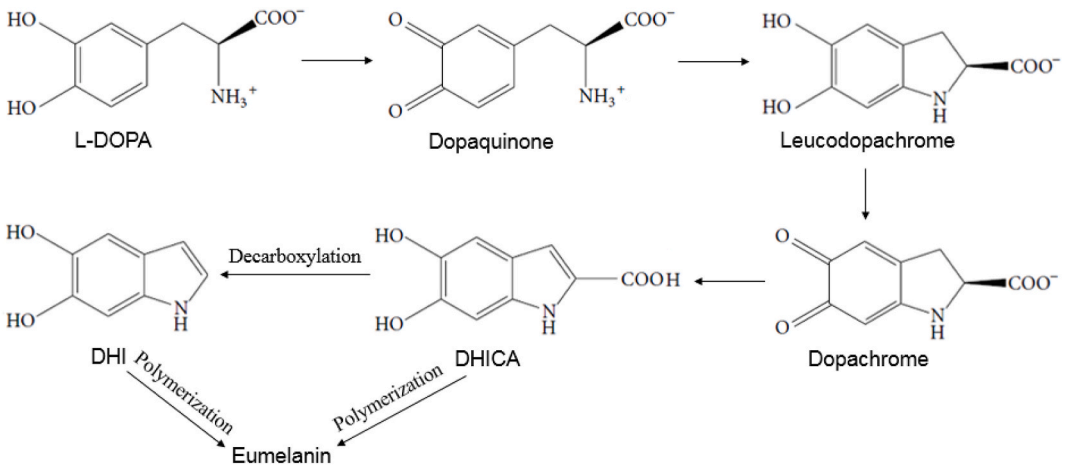

Fig. 1. Simplified schematic of the oxidative polymerization of L-DOPA.

2.4. Interfacial shear strength measurement

The interfacial shear strength (IFSS) was measured by using the single fibre fragmentation test (SFFT) to present the bonding strength of the composites in this study. Single fibre composites (SFCs) were prepared for the SFFT, which were cut into dog-bone specimens as described previously (Tan et al., 2018a). Ten repeats were processed for each subject. IFSS values (τ) were calculated using the Kelly-Tyson equation (Haque et al., 2010):

$$\tau = \frac{\sigma_f \cdot d}{2 \cdot l_c} \tag{1}$$

where d is the fibre diameter and σ_f is the single fibre tensile strength at the critical fragment length l_c determined by:

$$\sigma_f = \sigma_0 \cdot \left(\frac{l_c}{l_0}\right)^{-1/m} \tag{2}$$

$$l_c = \frac{4}{3} \cdot l_f \tag{3}$$

$$l_f = \frac{l_0}{N} \tag{4}$$

where σ_0 and m are the Weibull scale and shape parameter respectively for the fibre strength at gauge length l_0. Weibull shape and scale refer to Weibull modulus and normalising stress, respectively. Weibull normalising stress indicates the most probable stress at which a certain fibre will fail (Tan et al., 2018b). l_f is the average fragment length and N is the number of fibre fragments.

2.5. Statistical analysis

A Student's unpaired t-test was used to analyse the difference in fibre strength and IFSS between the coated PGF and the uncoated PGF control, assuming equal variance and determining two-tailed p values (Tan et al., 2017). It was performed using IBM SPSS (version 22) and a threshold value of 0.05.

3. Results

3.1. SEM analysis

The surface of the PDP-4 sample was visibly rougher than the other samples (PDP-0, PDP-0.5, PDP-1 and PDP-2) as seen in Fig. 2. An axial crack was observed on the surface of PDP-4, which was probably caused by a polymer shrinking after drying or incomplete coating layer. Additionally, no other evidence to indicate any surficial crack on the PGF itself after coating application.

3.2. TG analysis

Fig. 3a and b presents material loss of the samples in wt% during heating. A derivative of the wt% curve (DTG) is also presented for a further analysis of decomposition temperature. Normally, L-DOPA will decompose at 276–278 °C (Yamada et al., 1962). Fig. 3a shows that the L-DOPA powders in this study decomposed from ~278 °C. It also shows two distinct peaks at 303 °C and 366 °C, which is attributed to the degradation of different functional groups of L-DOPA. As shown as the TG curves in Fig. 3b, weight loss of different samples shows a clear trend following the L-DOPA concentration. Decomposition of the oxidative L-DOPA agent started from ~210 °C.

3.3. FTIR analysis

The spectrum of PDP-0 was taken as control and that of purchased L-DOPA powders was used as a reference during IR analyses. Five main peaks were found for the PDP-0 absorption bands as labelled in Fig. 4a, which were consistent with the literature (Tan et al., 2017). All of these five bands were also observed for PDP-0.5, 1, 2 and 4 without any significant positional difference. The band assignments are listed in Table 2.

The absorption bands corresponding to the aromatic structure of L-DOPA were expected to locate in the range between 1200 and 1700 cm^{-1}. The bands of L-DOPA at 1353, 1404, 1440, 1458, 1498 and 1527 cm^{-1} were observed to shift slightly to higher wavenumbers in PDP-4 as shown in Fig. 4b. Some new bands appeared in PDP-4 at 1513, 1552 and 1581 cm^{-1}. Moreover, the band of L-DOPA at 1652 cm^{-1} was replaced by three new bands at 1642, 1650 and 1658 cm^{-1} in PDP-4. Many other bands also appeared below 1200 cm^{-1} in PDP-4, but they were expected to be obscured by overlapping with the absorption bands of PGFs.

3.4. XPS analysis

High-resolution XPS spectroscopy was performed on uncoated and coated PGFs and L-DOPA powders. Narrow scans of C_{1s}, O_{1s}, N_{1s} and P_{2p} are exhibited in Fig. 5. The signal of L-DOPA powders in C_{1s} was resolved

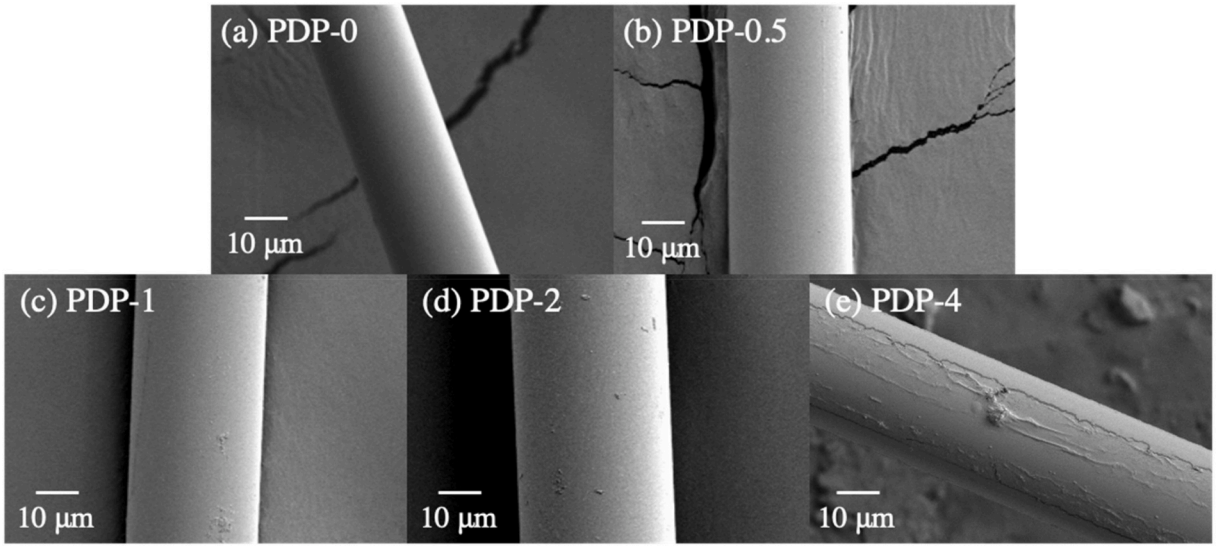

Fig. 2. Magnified images of uncoated and coated PGFs (Scale 1200:1). The cracked base shows the conductive tape.

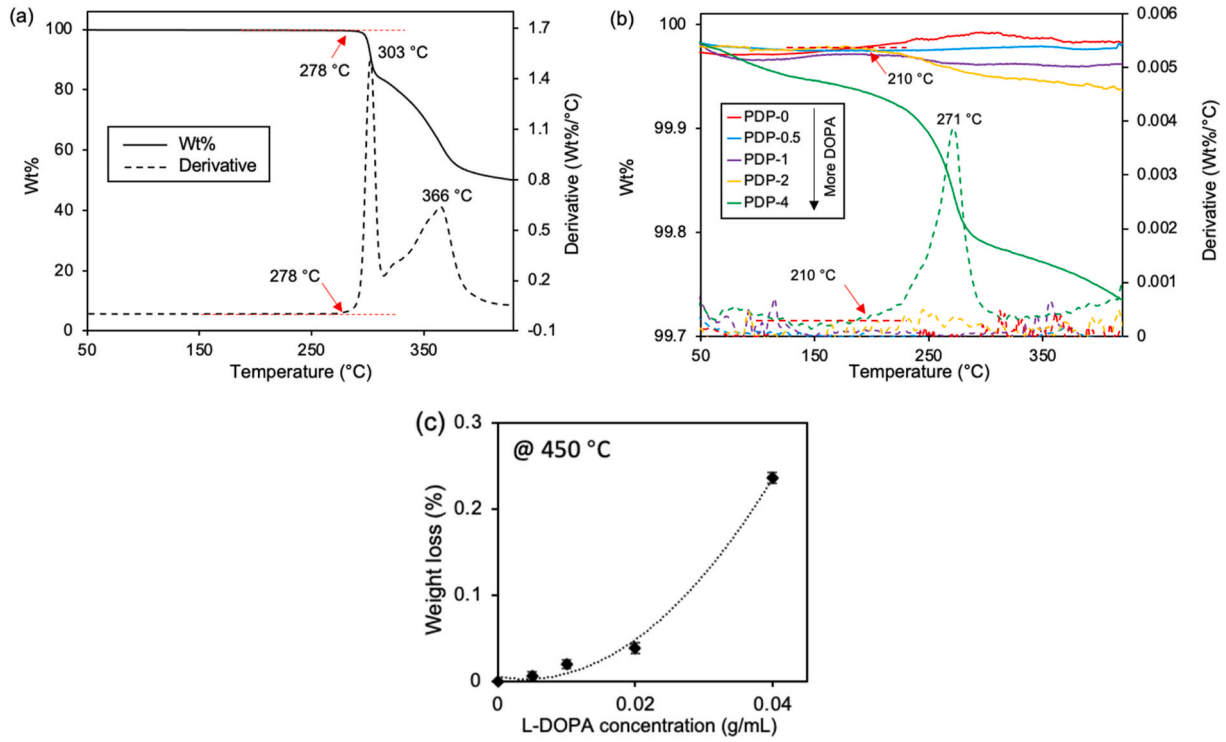

Fig. 3. TA analysis of (a) L-DOPA powders and (b) uncoated and coated PGFs; (c) Weight loss of coated PGFs after heating at 450 °C.

into three main components at 284.5, 285.8 and 288.7 eV binding energy. One more peak of very low intensity was observed at 291.4 eV. The peaks at 288.7 eV were also observed for PDP-0.5, 1, 2 and 4 with atomic percent of 8.9%–12.4%. The peak at 284.5 eV was found to slightly shift to the higher binding energy for all the coated samples.

The nitrogen peak of L-DOPA was resolved into two signals, involving a predominant one at 402.0 eV and another one at 399.8 eV binding energy. Their atomic ratio was 91:9. These two peaks were also found for PDP-0.5, 1, 2 and 4 with different atomic ratios.

The O_{1s} peak of PDP-0 required two peaks at 531.2 and 532.7 eV for the curve fit. The peak at 531.2 eV slightly shifted to a higher binding energy, wherein 531.2 eV for PDP-0.5, 1 and 4 and 531.4 eV for PDP-2. The peak at 532.7 eV remained for PDP-0.5, 1 and 2, but shifted to 532.6 eV for PDP-4. It was also observed that the ratio of peak at ~531.2 eV decreased from PDP-0.5 to PDP-4 with increasing L-DOPA concentration. The O_{1s} peak of L-DOPA was resolved into two peaks at 531.7 and 532.8 eV.

The P_{2p} peak of PDP-0 was deconvoluted into two peaks at 133.6 and 134.5 eV binding energy. Their atomic ratio was 67:33. Similar peaks were observed in the spectra for PDP-0.5 and 1. The peak pairs for PDP-2 and 4 slightly shifted to 133.7 and 134.6 eV.

3.5. Fibre strength analysis

No significant change was found for the modulus between the coated and uncoated PGFs from Fig. 6a. Tensile strength of PGFs are shown in Fig. 6b and Table 3. The table also presents the fibre diameters and Weibull parameters. As shown in Fig. 6b, all the PGF samples maintained tensile strength after coating application. The strength of PDP-4 is even significantly higher than all the other samples, which increased by 17.8% ($p < 0.01$) compared to the uncoated fibres.

It was observed from Table 3 that the trend of normalising strength was consistent with that of mean tensile strength. The Weibull modulus of the PGFs ranged between 4.4 and 6.0. Fig. 6c shows an example of the Weibull plots. The fibre diameters were around 27 μm and no significant change in diameter was observed between coated and uncoated PGFs.

3.6. IFSS analysis

As shown in Fig. 7, all the coated samples show a higher IFSS value compared to PDP-0. PDP-1 shows the best coupling performance, which increased by 27% ($p < 0.001$) compared to PDP-0. However, the coupling performance dropped back down when L-DOPA concentration further increased to PDP-2 and kept at ~5.5 MPa level for PDP-4.

4. Discussion

4.1. FTIR analysis

IR spectroscopy for coated PGFs compared to that of uncoated PGFs and L-DOPA powders to detect the existing and chemical change of coating agent on the PGF surface. As shown in Fig. 4a, the five main bands for PDP-0 were also found for PDP-0.5, 1, 2 and 4, which indicated that the intrinsic phosphate structure was not destroyed/altered during coating.

Fig. 4b shows the main bands for L-DOPA. The bands at 1353, 1440, 1498 and 1565 cm^{-1} were attributed to the vibration of ring deformation (Mazur et al., 2013), which slightly shifted towards higher wavenumbers for PDP-4, due to a formation of the quinone groups and an indole structure on the ring. This is also evidenced by XPS results. The bands at 1249 and 1282 cm^{-1} assigned to the bending and stretching modes of the phenolic groups respectively (Mazur et al., 2013), did not change in PDP-4, indicating remaining hydroxyl groups on the ring. The crosslink reactions between the hydroxyl and quinone forms lead to the polymerization of the oxidized L-DOPA (Quan et al., 2019). Moreover, the shifts of these bands in PDP-4 might also be attributed to the weak interactions, such as Van der Waals forces and hydrogen bridges between the L-DOPA and the hydroxyl groups on PGF surface.

The bands of 1404 and 1458 cm^{-1} were attributed to the bending vibrations of the methylene (Sukker et al., 2015), which shifted to higher wavenumbers for PDP-4, due to the formation of DHICA, where the $–CH_2–$ group has changed into –CH = .

The band at 1527 cm^{-1} assigned to the bending vibration of amino

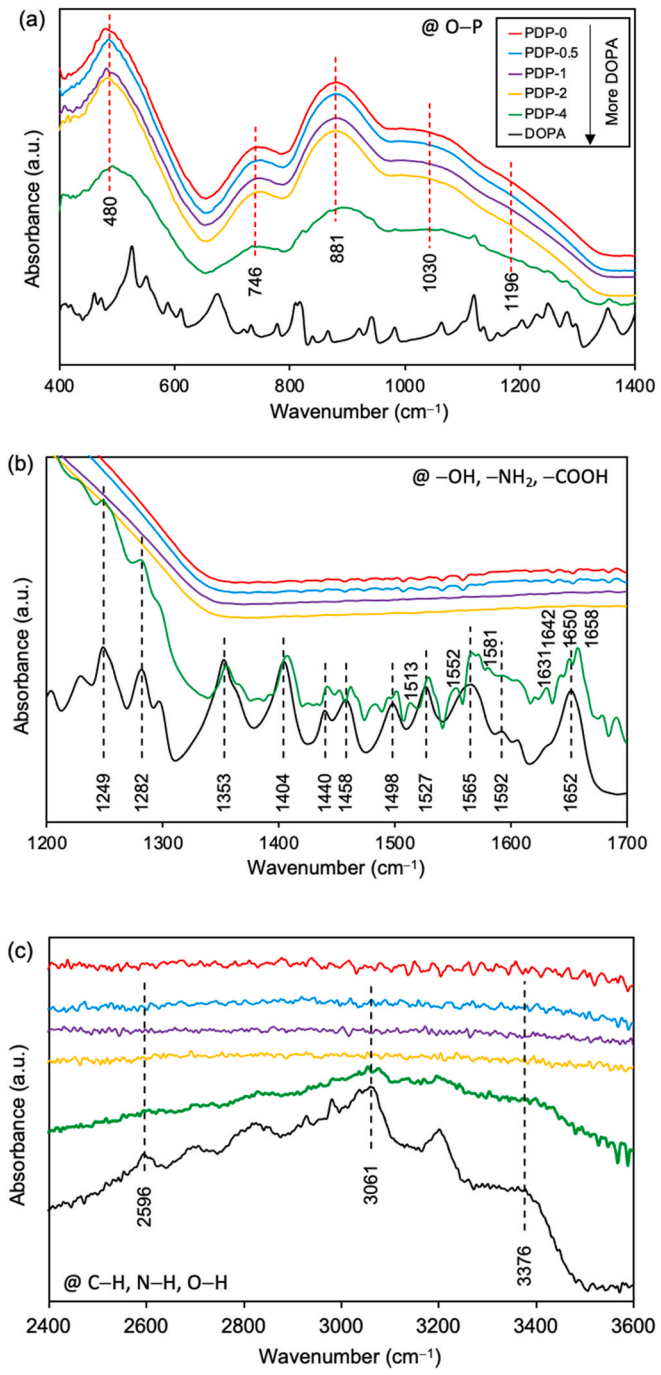

Fig. 4. FTIR spectra to show the main absorption bands for (a) PGFs and (b, c) the functional groups of L-DOPA.

groups (Lin et al., 2015) slightly shifted to a higher wavenumber for PDP-4 with the appearance of a new band at 1513 cm^{-1}, due to the interaction between the L-DOPA and PGFs. Lin et al. (2015) added L-DOPA agents for graphene-chitosan composites and found the $–NH_2$ absorption band shifted from 1526 to 1518 cm^{-1}, which was suggested to be due to the chemical binding between the L-DOPA and chitosan.

The appearance of the band at 1631 cm^{-1} might come from the C═C stretching vibration of indole, speculating the intramolecular cyclization reaction of L-DOPA to form the indole derivatives (Yu et al., 2010).

The weak band at 1592 cm^{-1} and the intense band at 1652 cm^{-1} were attributed to the C–N bend of the protonated amine group and the C═O stretch of the deprotonated carboxylic group respectively (Jaber et al., 2011), existing as a zwitterion in L-DOPA (Jaber et al., 2011). In

Table 2
FTIR band assignments for pure PGF and L-DOPA.

Wavenumber (cm^{-1})	Assignments	Ref.
PGF		
480	δ_{as}(O–P–O) in Q^1 species	Lu et al. (2015)
746, 881	ν_s and ν_{as}(P–O–P) of the bridging oxygen in Q^2 species	Sharmin et al. (2016)
~1030	ν_s and ν_{as}($P–O^-$) in Q^1 species	Sharmin et al. (2016)
~1196	$\nu_{as}(PO_2)^-$ of the non-bridging oxygen in Q^2 species	(Lu et al., 2015; Sharmin et al., 2016)
L-DOPA		
1249, 1282	δ and ν(C–OH) of the phenolic groups	(Jaber et al., 2011; Mazur et al., 2013)
1353, 1440, 1498, 1565	Ring deformation vibration	(Jaber et al., 2011; Mazur et al., 2013; Sukker et al., 2015)
1404, 1458	$\delta(-CH_2-)$ of the methylene	Sukker et al. (2015)
1527	$\delta(C–NH_2)$	Lin et al. (2015)
1592	$\delta(C–NH_3^+)$	Jaber et al. (2011)
1652	ν(C═O) of $–COO^-$	Weinhold et al. (2006)
2500–3050	Different C–H vibrations of either aromatic or aliphatic C–H bonds	(Jaber et al., 2011; Mazur et al., 2013; Sukker et al., 2015)
3051–3500	ν(N–H) and ν(O–H)	(Jaber et al., 2011; Mazur et al., 2013; Sukker et al., 2015)

*δ_s (δ_{as}) = symmetric (asymmetric) bending vibration.
**ν_s (ν_{as}) = symmetric (asymmetric) stretching vibration.

comparison, the band at 1592 cm^{-1} was still observed in PDP-4 and partially superposed with a band at 1581 cm^{-1} assigned to the bending vibration of $–NH_2$ (Lawrie et al., 2007). Another new band was observed at 1552 cm^{-1} for PDP-4, due to one of the $–NH_3^+$ vibrational modes (Lawrie et al., 2007). Three new bands appeared at 1642, 1650 and 1658 cm^{-1} in PDP-4 instead of the band at 1652 cm^{-1} in L-DOPA, which was related to the appearance of C═O in quinones and the reactional behaviour of –COO– groups (Weinhold et al., 2006). Jaber et al. (2011) investigated bulk L-DOPA and L-DOPA composites (DOPA-aerosil, DOPA-saponite and DOPA-laponite) by FTIR. They reported that the band at 1758 cm^{-1} was assigned to the carboxylic C═O stretch of the protonated –COOH and the absence of this band indicated the deprotonation of the carboxylic acid in the spectra of L-DOPA and its composites. Therefore, they stated that the $–NH_3^+$ group of L-DOPA (or its polymerization products) presents as a zwitterion to keep the equilibrium, but not a cation.

The bands at 2596-3050 cm^{-1} shown in Fig. 4c were attributed to different C–H vibrations of either aromatic or aliphatic C–H bonds, while the bands at 3061-3376 cm^{-1} were due to a superposition of stretching vibrations of N–H and O–H (Jaber et al., 2011; Mazur et al., 2013; Sukker et al., 2015).

4.2. XPS analysis

XPS was used to investigate chemical interaction between L-DOPA and PGF surface. As shown in Fig. 5a, the C_{1s} peak of L-DOPA was fitted as $C–C/CH_x$ at 284.5 eV (C1, 4, 5, 6, 7), C–N/C–OH at 285.8 eV (C2, 3, 8) and –COO– at 288.7 eV (C9) (Jaber et al., 2011; Weinhold et al., 2006). Theoretical atomic ratio of the three main peaks is 56:33:11, while the experimental result is 55:36:9, which shows a good consistency. The three peaks were also resolved from the C_{1s} peaks of PDP-0.5, 1, 2 and 4, indicating the presence of L-DOPA on PGF surface. However, the binding energies and atomic ratios of these components showed distinct changes when compared to those of neat L-DOPA. The peak at 284.5 eV shifted to 284.8 ± 0.1 eV and the atomic percentage (atom%) of the peak at 285.7 ± 0.2 eV increased from 35.6% to 43.6%, which was attributed to formation of the indole structure (Weinhold et al., 2006). A significant increase in atom% of the peak at 288.7 eV was observed for coated PGF

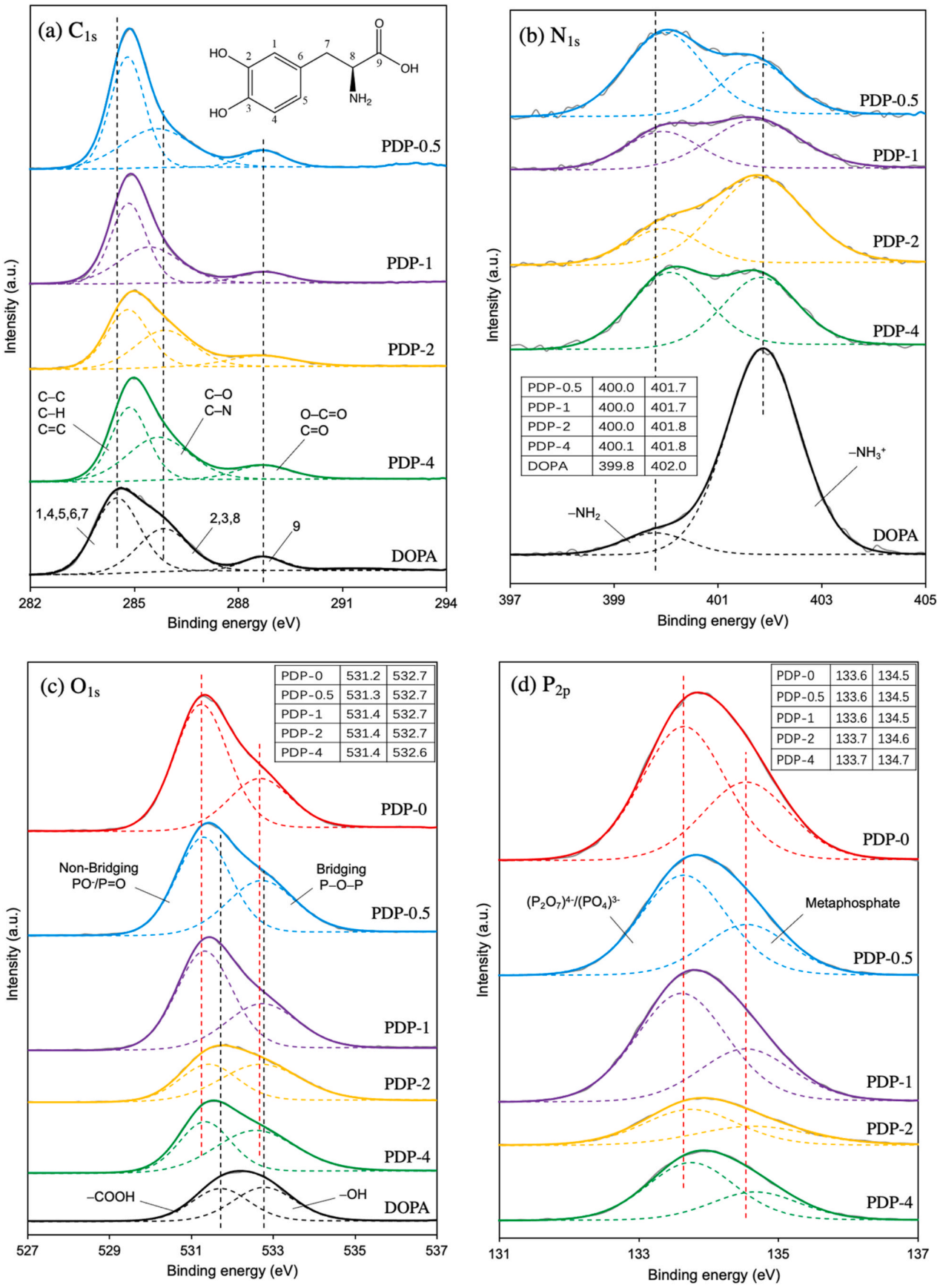

Fig. 5. XPS spectra of (a) C_{1s}, (b) N_{1s}, (c) O_{1s} and (d) P_{2p} narrow scans of L-DOPA powders and uncoated and coated PGFs.

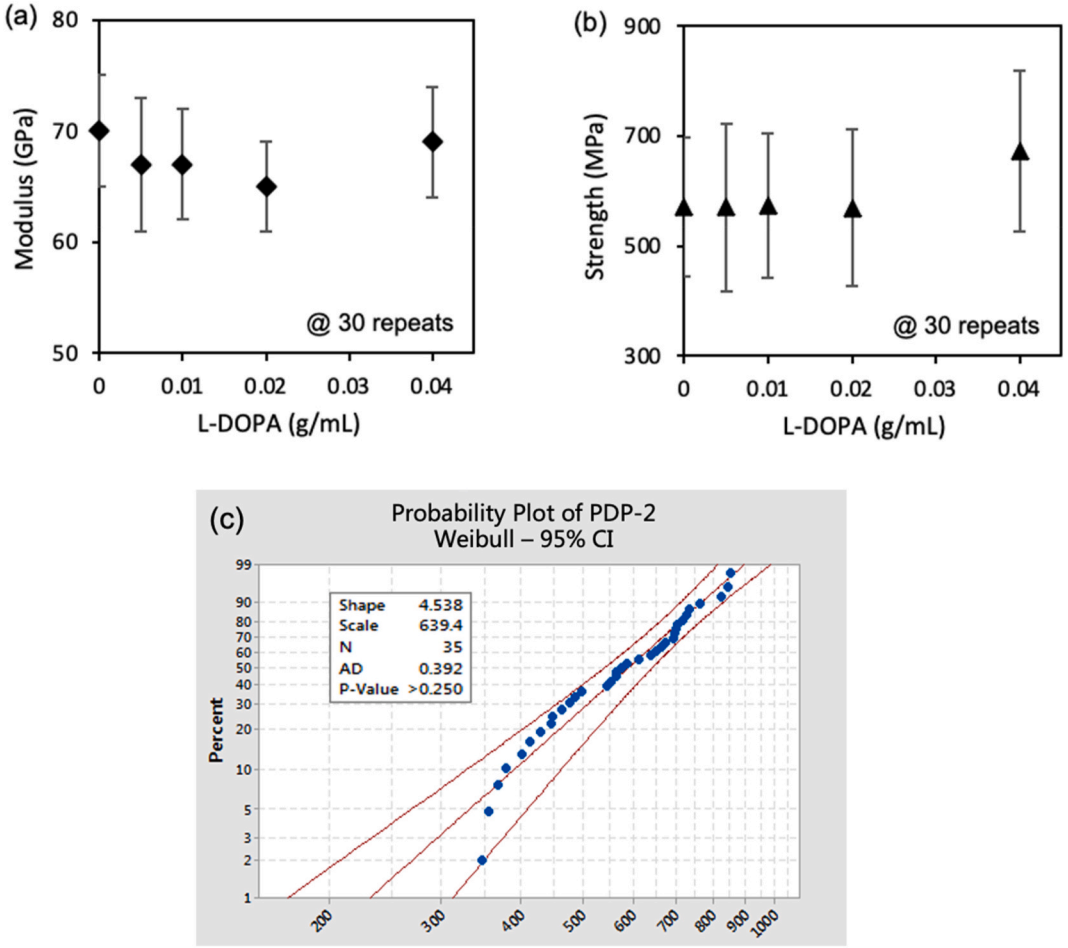

Fig. 6. (a) Tensile modulus and (b) strength of uncoated and coated PGFs. (c) Weibull analysis for PDP-2 plotted by Minitab.

Table 3
Diameters and Weibull parameters of uncoated and coated PGFs ($n = 30$).

Sample codes	Diameter (μm)	Tensile strength (MPa)	Normalising strength (MPa)	Weibull modulus
PDP-0	27 ± 2	571 ± 126	620	5.5
PDP-0.5	28 ± 1	570 ± 153	627	4.4
PDP-1	28 ± 1	573 ± 132	626	4.6
PDP-2	27 ± 2	569 ± 143	624	4.5
PDP-4	27 ± 1	673 ± 147	729	6.0

samples compared to L-DOPA, which was attributed to appearance of quinone groups (Liebscher et al., 2013). These are also evidenced by FTIR results.

The N_{1s} peak of L-DOPA has a predominant component at 401.9 eV (atom% = 91.1%) assigned to R–NH_3^+ and a minor sub-peak of R–NH_2 at 399.8eV (atom% = 8.9%). The predominance of protonated amine was due to the zwitterion structure of L-DOPA (Jaber et al., 2011). In analogy with glycine, L-DOPA is more stable as a zwitterionic ($^+NH_3$–CHR–COO^-) rather than a neutral (NH_2–CHR–COOH) form in aqueous solution (Jaber et al., 2011). Jaber et al. (2011) also reported observation of the L-DOPA zwitterion in XPS. They suggested this was as a result of water trapped in the L-DOPA crystal. In this case, the formation of indole structure broke the zwitterionic-neutral equilibrium of L-DOPA, which led to that the peak at 399.8 eV shifted to 400.0 ± 0.07 eV and the peak at 401.9 eV shifted to 401.8 ± 0.06 eV.

The O_{1s} spectrum of PGF was deconvoluted into two peaks at 531.2 and 532.7 eV, assigned to P–O/P═O non-bridging (NBO) and P–O–P bridging (BO) phosphate oxygens, respectively (Felfel et al., 2021; Haque et al., 2010). As shown in Fig. 5c, the peak of NBO at 531.2 eV slightly shifted to a higher binding energy. It indicated a new connection instead of that between the NBO and the metal ion in the glass, which

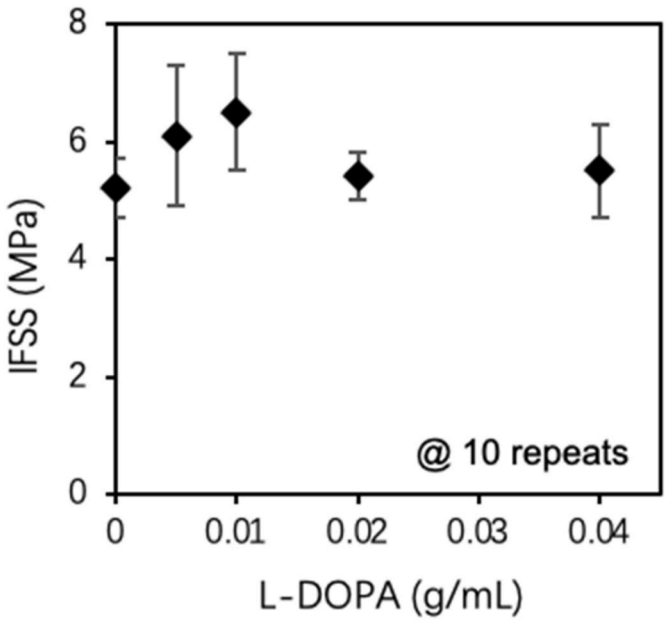

Fig. 7. Interfacial shear strength obtained from fragmentation tests.

was suggested to be a bidentate bonding between the glass surface hydroxyl oxygen and the catechol groups from L-DOPA (Ye et al., 2011). The decrease in ratio of NBO/BO from PDP-0 to PDP-4 also indicated the reduction of hydroxyl groups on the PGF surface. Messersmith et al. (Dalsin et al., 2005) reported such a binding mechanism between the hydroxyl groups on TiO_2 surface and the catechol groups from L-DOPA.

The O_{1s} spectrum of L-DOPA was resolved into two peaks at 531.7 and 532.8 eV, assigned to the oxygen of the carboxyl and hydroxyl groups, respectively (Weinhold et al., 2006). Theoretical oxygen atomic ratio of the –COO– and –OH is 50:50, while the experimental value is 47:53, which was due to the water trapped in the L-DOPA crystal.

The P_{2p} spectrum of PGF was composed of the $P_{2p3/2}$/$P_{2p1/2}$ doublet and fitted with an energy difference of 0.9 eV and an approximate atomic ratio of 2:1. The peak of $P_{2p3/2}$ at 133.6 eV was attributed to pentavalent tetra coordinated phosphorus (pyrophosphate and orthophosphate) surrounded by a different chemical environment (phosphate-like structure) and the peak of $P_{2p1/2}$ at 134.5 eV was attributed to metaphosphate (Parsons et al., 2019). Similar peaks were observed in the spectra for PDP-0.5 and 1. The phosphate peak doublet slightly shifted to a higher binding energy for PDP-2 and 4, which was attributed to the sufficient binding between the glass and the L-DOPA agent. It indicated a sufficient chemical linking to influence the phosphate surface structure. Moreover, it is also shown in Fig. 5d that the spectral intensity of PDP0.5 and 1 is lower than that of PDP-0, while that of PDP-2 and 4 is obviously further lower. This observation is ascribed to the depth penetration observed for XPS (ca. 5–10 nm) (Felfel et al., 2021), which indicated a nano-scaled coating layer for the PGFs. This was also observed from the oxygen peaks (Fig. 5c).

4.3. Fibre strength analysis

The influences of L-DOPA coating on mechanical properties of PGFs were investigated by a comparison of coated PGFs with the control PDP-0. As shown in Fig. 6a, no significant change in the tensile modulus was observed from different samples, indicating that the intrinsic glass structure was conserved after coating application. L-DOPA did not contribute significantly to the fibre modulus, since it has a much lower modulus than the glass.

Fig. 6b shows that the tensile strength of PDP-0.5, 1 and 2 remained almost constant compared to PDP-0, suggesting that the 30 min immersion in the coating solution at these concentrations did not have a significant effect on the mechanical strength of the PGFs. However, the strength of PDP-4 is significantly higher than all the other samples, which increased by 17.8% ($p < 0.01$) compared to PDP-0. It is suggested that the increase in the strength of PDP-4 was as a result of a much thicker coating of L-DOPA. This is consistent with the observation from SEM, TGA and spectroscopy, where PDP-4 showed a significant difference when compared to the other samples. The strength of the glass fibre heavily depends on the critical flaws locating at the fibre surface, so the fibre fracture behaviour is strongly affected by the coating properties (Gao et al., 2008, 2011). Herein, we suggest that the PDP-4 coating protected the fibre surface from abrasion and surface flaw formation during handling operations, as well as leading to reduction of moisture contact and surface reactions (Gao et al., 2011).

4.4. IFSS analysis

As shown in Fig. 7, all the coated samples show a higher IFSS value compared to PDP-0. The IFSS of PDP-0.5 increased by 19% compared to PDP-0, which also shows an instable performance compared to other sample sets. This might be due to there being insufficient L-DOPA available or poor dispersion in the solution to fully and uniformly coat the PGFs. The IFSS of PDP-1 increased by 27% of the control, which was significant ($p < 0.001$), suggesting that there was sufficient L-DOPA available to generate interactions between the L-DOPA-coating and the PGF surface.

Phosphate glass immersed in aqueous solution generate $–O^-$ groups at the glass surface due to the rapid release of sodium ions, which are proton acceptors (Kohl et al., 2017). Meanwhile, the catechol and amine groups from L-DOPA are competing as proton donors (Yang et al., 2011). Therefore, strong hydrogen bonding is anticipated to occur between the PGF surface and L-DOPA. Kohl et al. (2017) reported that glass fibres with native surface hydroxyl groups can have strong hydrogen bonding interactions (high surface energy) with polar functional groups of the polymers in glass fibre reinforced composites. A bidentate bonding between the glass surface hydroxyl oxygen and the catechol groups from L-DOPA was considered for PDP-0.5, 1, 2 and 4, as described for the O_{1s} spectrum of PGF in XPS Discussion. Besides, a binding between the hydroxyl oxygen on PGF surface and the amine group from L-DOPA was considered for PDP-4, which was evidenced by the FTIR band appeared at 1513 cm^{-1}.

However, the performance of L-DOPA coating on IFSS weakened for PDP-2 and 4, as shown in Fig. 7. It may relate to the formation and growth of the melanin-like polymer layer, which consumed the active groups of L-DOPA in turns weakening the interaction with the PGF surface and reducing the efficiency of load transmission from the matrix to the PGFs. As mentioned above, the catechol and amine groups from L-DOPA are competing as proton donors. When the L-DOPA concentration is too low to polymerize and crosslink, the monomeric L-DOPA prefers to attach to the PGF surface with the catechol groups (Yang et al., 2011). As the concentration increases, the oxidized L-DOPA is inclined to polymerize mainly based on the crosslink reactions between the hydroxyl and quinone forms (Liebscher et al., 2013). That is, the bulk of catechol groups of the L-DOPA are consumed and the amount of the amine groups becomes higher than that of the catechol groups, which turns to the main proton-donors (Yang et al., 2011). However, the formation of indole structure consumes the amine groups, which also limits the connection between the coating agent and the PGF.

Therefore, optimum conditions for fibre strength and for IFSS do not coincide and so an optimum must be selected based on application. Where only coated fibres are used, as for example a filter or other textile application, a thicker coating of at least 4% L-DOPA solution (PDP-4) should be used to maximise strength. Where IFSS is critical, for example in a polymer composite intended for long term degradation, an optimum coating of 1% L-DOPA solution (PDP-1) should be selected.

5. Conclusions

This study showed that the L-DOPA agent at different concentrations can significantly improve the IFSS of PGF/PCL composites (at conc. of 10 g L^{-1}) and the tensile strength of the glass fibres (at conc. of 40 g L^{-1}). SEM and TGA analyses confirmed that the concentration of L-DOPA solution affected the coating thickness. In the interface bonding mechanism FTIR and XPS spectroscopy data showed that the catechol and amine groups of L-DOPA were competing as proton donors, whilst the hydroxyl oxygen group at the glass fibre surface acted as proton acceptor. At low L-DOPA concentrations polymerization and crosslinking were affected, as the monomeric L-DOPA preferred to bind with the glass fibre via the catechol groups. As the concentration increased, the L-DOPA agent would bind with the glass fibre via the amine groups and the cross-linked precipitation. The results obtained showed that an optimum coating level could be tailored dependent on application and whether fibre strength or IFSS was of greater importance or priority.

CRediT authorship contribution statement

Chao Tan: Writing – original draft, Visualization, Validation, Methodology, Investigation, Data curation, Conceptualization. **Chris D. Rudd:** Writing – review & editing, Supervision, Project administration, Funding acquisition. **Andrew J. Parsons:** Writing – review & editing, Visualization, Methodology. **Nusrat Sharmin:** Writing – review & editing, Visualization. **Ifty Ahmed:** Writing – review & editing,

Supervision, Methodology, Funding acquisition.

Declaration of competing interest

The authors declare that they have no known competing financial interests or personal relationships that could have appeared to influence the work reported in this paper.

Data availability

Data will be made available on request.

Acknowledgements

The author would like to acknowledge the financial support from the International Doctoral Innovation Centre (IDIC) of the University of Nottingham, the EPSRC (Grant No. EP/L016362/1) and the Sichuan Science and Technology Foundation (2022YFSY0045).

References

Ambrosi, T.H., et al., 2021. Aged skeletal stem cells generate an inflammatory degenerative niche. Nature 597, 256–262.
Cheng, B., et al., 2022. Ultrastrong underwater adhesion on diverse substrates using non-canonical phenolic groups. Nat. Commun. 13 (1), 1892.
Dalsin, J.L., Lin, L., Tosatti, S., Voros, J., Textor, M., Messersmith, P.B., 2005. Protein resistance of titanium oxide surfaces modified by biologically inspired mPEG-DOPA. Langmuir 21, 640–646.
Felfel, R.M., Parsons, A.J., Chen, M., Stuart, B.W., Wadge, M.D., Grant, D.M., 2021. Water resistant fibre/matrix interface in a degradable composite: synergistic effects of heat treatment and polydopamine coating. Compos. Part A-Appl. S. 146.
Gao, S., Mader, E., Plonka, R., 2008. Nanocomposite coatings for healing surface defects of glass fibers and improving interfacial adhesion. Compos. Sci. Technol. 68 (14), 2892–2901.
Gao, S.-L., Zhang, J., Liu, J.-W., Zhuang, R.-C., Plonka, R., Mäder, E., 2011. Healing microcracks and early warning composite fractures. In: Presented at the 6th Colloquium on Textile Reinforced Structures. CTRS6), Berlin.
Haque, P., et al., 2010. Interfacial properties of phosphate glass fibres/PLA composites: effect of the end functionalities of oligomeric PLA coupling agents. Compos. Sci. Technol. 70 (13), 1854–1860.
Jaber, M., Bouchoucha, M., Delmotte, L., Méthivier, C., Lambert, J.-F. o., 2011. Fate of L-DOPA in the presence of inorganic matrices: vectorization or composite material formation? J. Phys. Chem. C 115 (39), 19216–19225.
Jo, Y.K., Kim, H.J., Jeong, Y., Joo, K.I., Cha, H.J., 2018. Biomimetic surface engineering of biomaterials by using recombinant mussel adhesive proteins. Adv. Mater. Interfac. 5 (9).
Kohl, J.G., Malicky, D.M., Jones, A.M., 2017. Adhesion of epoxy (pseudobarnacles) to glass that has been treated with hydrophobic carbosilane-based coatings. Prog. Org. Coating 107, 1–4.
Lawrie, G., et al., 2007. Interactions between alginate and chitosan biopolymers characterized using FTIR and XPS. Biomacromolecules 8, 2533–2541.
Lee, H., Lee, B.P., Messersmith, P.B., 2007. A reversible wet/dry adhesive inspired by mussels and geckos. Jul 19 Nature 448 (7151), 338–341.
Lee, K., Oh, M.H., Lee, M.S., Nam, Y.S., Park, T.G., Jeong, J.H., 2013. Stabilized calcium phosphate nano-aggregates using a dopa-chitosan conjugate for gene delivery. Mar 10 Int. J. Pharm. 445 (1–2), 196–202.
Lee, H.A., Ma, Y., Zhou, F., Hong, S., Lee, H., 2019. Material-independent surface chemistry beyond polydopamine coating. Mar 19 Acc. Chem. Res. 52 (3), 704–713.
Liebscher, J., et al., 2013. Structure of polydopamine: a never-ending story? Aug 20 Langmuir 29 (33), 10539–10548.
Lin, L., Lian, H.-T., Sun, X.-Y., Yu, Y.-M., Liu, B., 2015. An L-dopa electrochemical sensor based on a graphene doped molecularly imprinted chitosan film. Anal. Methods-UK 7, 1387–1394.
Lin, X., et al., 2020. Phosphate glass fibers facilitate proliferation and osteogenesis through Runx2 transcription in murine osteoblastic cells. J. Biomed. Mater. Res. A 108 (2), 316–326.
Lu, M., Wang, F., Liao, Q., Chen, K., Qin, J., Pan, S., 2015. FTIR spectra and thermal properties of TiO_2-doped iron phosphate glasses. J. Mol. Struct. 1081, 187–192.
Mazur, M., et al., 2013. Iron oxide magnetic nanoparticles with versatile surface functions based on dopamine anchors. Apr 07 Nanoscale 5 (7), 2692–2702.
Parsons, A.J., Felfel, R.M., Wadge, M.D., Grant, D.M., 2019. Improved phosphate-based glass fiber performance achieved through acid etch polydopamine treatment. Int. J. Appl. Glass Sci. 11 (1), 35–45.
Quan, W.Y., et al., 2019. Mussel-Inspired catechol-functionalized hydrogels and their medical applications. Molecules 24 (14).
Sharmin, N., et al., 2016. Effect of boron oxide addition on the viscosity-temperature behaviour and structure of phosphate-based glasses. J. Biomed. Mater. Res. B 105 (4), 764–777.
Sukker, G.M., Wazzan, N., Hilal, R., 2015. Towards understanding mode of action of L-dapa and carbidopa: DFT/TD-DFT analyses of their electronic and vibration spectra. Indian J. Chem. 54A, 1378–1386.
Tan, C., et al., 2017. Structural, thermal and dissolution properties of MgO- and CaO-containing borophosphate glasses: effect of Fe_2O_3 addition. J. Mater. Sci. 52, 7489–7502.
Tan, C., et al., 2018a. Chitosan as a coupling agent for phosphate glass fibre/polycaprolactone composites. Fibers 6 (4), 97–121.
Tan, C., et al., 2018b. Effects of Fe2O3 addition and annealing on the mechanical and dissolution properties of MgO- and CaO-containing phosphate glass fibres for bio-applications. Biomed. Glasses 4 (1), 57–71.
Weinhold, M., et al., 2006. Structure and bonding of the multifunctional amino acid L-DOPA on Au(110). J. Phys. Chem. B 110 (47), 23756–23769.
Yamada, S.-i., Fujii, T., Shioiri, T., 1962. Studies on optically active amino acids. III. Preparation of 3-(3, 4-Dihydroxyphenyl)-DL-, -D-, and -L-alanine. Chem. Pharm. Bull. 10 (8), 693–697.
Yang, L., et al., 2011. A biomimetic approach to enhancing interfacial interactions: polydopamine-coated clay as reinforcement for epoxy resin. Aug ACS Appl. Mater. Interfaces 3 (8), 3026–3032.
Ye, Q., Zhou, F., Liu, W., 2011. Bioinspired catecholic chemistry for surface modification. Jul Chem. Soc. Rev. 40 (7), 4244–4258.
Yu, F., et al., 2010. Experimental and theoretical analysis of polymerization reaction process on the polydopamine membranes and its corrosion protection properties for 304 Stainless Steel. J. Mol. Struct. 982 (1–3), 152–161.